12th International Conference on Fracture Mechanics of Concrete and Concrete Structures
FraMCoS-12
B.L.A. Pichler, Ch. Hellmich, P. Preinstorfer (Eds)

https://doi.org/10.21012/FC12.1362
TT-E:2

IDENTIFYING INTERLAYER FRACTURE PROPERTIES IN 3D PRINTED CONCRETE SPECIMENS VIA MULTIDIRECTIONAL FLEXURAL TESTS

K. SRIRAM KOMPELLA[*], MARINELLA LEVI[†] AND LIBERATO FERRARA[*]

[*] Politecnico di Milano, Dipartimento di Ingegneria Civile e Ambientale
Piazza Leonardo da Vinci, 32, Milano 20133, Italy
e-mail: kasyapasriram.kompella@polimi.it

[†] Politecnico di Milano, Dipartimento di Chimica, Materiali e Ingegneria Chimica "Giulio Natta"
Piazza Leonardo da Vinci, 32, Milano 20133, Italy

Key words: Concrete 3-D printing, influence of layers, flexural strength and fracture energy, numerical modelling, experimental validation

Abstract: 3D printing of concrete presents the new challenge of anisotropy to an already heterogenous medium of concrete. The layer-wise mode of construction quintessential to the printing of concrete leaves interfaces which have different properties to that of the layer. These interfaces interact and interfere with crack propagation compared to monolithically cast specimens and contribute to differential properties of structural elements in different directions. This phenomenon is identified by performing 3-point bending tests on printed elements with different layer orientations and comparing the fracture energy in Mode I (G_f) and peak flexural stresses (σ_f) of the printed concrete tested. Subsequently, ABAQUS model of 3-point bending tests are developed with different material properties of the interface elements and the layers which are validated against the experimental results. Upon parametrisation of the fracture energy and peak flexural stress values, it has been noted that the properties of the interface elements are categorised by the tests done with the loading direction parallel to the layer orientation.

1 INTRODUCTION

Given the novelty of the concrete 3D printing technology (C3DP), the structural design of printed structures is still an understudied area. With form-free fabrication made possible with the use of C3DP several benefits such as material savings and faster construction are unlocked. However, most current applications of this emergent technology remain non-structural due to the lack of studies of meso-scale and macro scale engineering structural properties of the printed concrete elements. One of such important structural phenomena is the anisotropy or more specifically the orthotropy of structural elements formed using the layer-wise additive manufacturing process [1,2]. The early age properties of a printable cementitious material are known to impact the hardened state properties through phenomenon like the presence of cold-joint like interfaces between layers. Given the complexity of printing processes, the involvement of additional parameters such as the printing speed, printing path, extrudability and buildability of the mix, open time of a given mix, the strength characteristics of the interfaces can vary significantly within a given a printed element despite having the exact same material

composition and age [3-6].

While there are no effective standards to study the bond between layers in printed concrete, several studies have been taken up to understand the effect of orthotropy and other interface related effects as part of the literature. The structural orthotropy of printed elements can be studied by understanding the influence of layer orientation on crack-propagation in Mode I fracture across layers. [7-10]. This study focusses on the understanding of the inter-layer bond in printed concrete elements by examining the Mode I fracture response in 3-point bending tests of printed elements of 160 mm × 25 mm × 40 mm with different layer orientations. Specimens were tested with layers parallel and perpendicular to the direction of loading. Specimens were also taken from the top and bottom of the printed element to understand different compaction of layers. Companion monolithically cast specimens were also tested similarly. The specimens with a lower compaction due to self-weight were registered as "top specimens", specimens with a higher compaction due to self-weight were registered as "bottom specimens", the specimens with layers orientation parallel to the direction of testing were registered as "vertical specimens" and specimens that were monolithically cast were tested as "cast specimens". The experimental results are then used for the development of an ABAQUS based finite element model as described further below.

2 EXPERIMENTAL METHODOLOGY AND ANLYSIS OF RESULTS

The mix design of the printable cementitious mortar was achieved after an iterative procedure. As can be expected, the mortar has a high proportion of binder. The special binder used is a blend of White 52.5 R CEM I cement (92%) and Calcium Sulfo Aluminate cement (8%) to achieve a fast-setting property. No specific set retarders or accelerators have been employed in this mix to ensure printability. The maximum aggregate size in the current mix is 0.6 mm which is that of ground recycled glass. The rest of the matrix is composed of Silica sand and quartz glass fine compound. Basalt fibres which are 16 mm in length and 13 μm in diameter have been used to ensure the cohesiveness required in the fresh state and avoid plastic shrinkage related defects. The basalt fibres had a tensile strength of 2800 MPa and an elastic modulus of 84 GPa. The proportion of 20 kg/m3 is equivalent to 0.7% V/V concentration in the cementitious composite upon homogeneous fibre dispersion. A water - binder ratio has been 0.295 to ensure adequate strength, together with 2.8% by weight of binder of a polycarboxylate ether-based superplasticiser to enhance workability, . The resulting mix had a 28-day compressive strength of about 70 MPa.

Rectangular prismatic specimens were extruded at 50 mm/min up to a height of 450 mm and lengths of 2000 mm from which specimens of mentioned heights and depths are cut with 10 mm notch depth and 4 mm width. These notches were made on all the specimens to localise cracking during the 3-point bending tests. Clips that can accommodate a clip-gauge were then glued to either side of the notch 4 mm apart. A clip-gauge connected to an electromechanical Instron machine with a range of 3 mm was then fitted to these clips. 3-point bending tests are then performed using crack-width control at a rate of 0.015 mm/s. The load was noted every 0.02 seconds until failure. The setup of the 3-point bending test can be seen below in Fig 1. The load vs COD curves of individual specimens with different layer orientations is plotted. The peak load registered in the 3-point bending test is then used to compute the peak flexural stress capacity of each individual specimen using the formula below where *l, b & d* are the dimensions of the specimens:

$$\sigma_f = \frac{3F_{max}l}{2bd^2} \quad (1)$$

The peak flexural stress thus calculated for all the specimens of similar dimensions are averaged together and are presented in the form of bar graphs in Fig 2. represented below. The

error bars depicted in the following figures are used solely to represent the maximum and minimum values of the flexural strength in MPa. It can be seen that the values of peak flexural capacity are similar for the printed elements tested with layer orientations perpendicular to the direction of loading and these are similar to that of the monolithically cast specimens. This indicates that the printing process has minimal effect on the flexural capacity in the direction perpendicular to the layer orientation. Whereas the vertical specimens reached only 45% of the flexural capacity of the printed specimens with layers perpendicular to the direction of loading. This indicates a clear orthotropy and the presence of weak interfaces between the layers.

The average load vs COD curves of specimens of different layer orientations have been calculated for different specimens of the same category by normalising the abscissa and ordiate values with respect to their local maxima and averaging the resultant normalised values. These curves are plotted for different categories of specimens as shown below in Fig 3. This is indicative of their overall mechanical performance. It can be seen that the vertical specimens were much weaker compared to the specimens with layer orientation perpendicular to the direction of loading. It can also be seen that the printed specimens have a very similar mechanical performance to that of the cast specimens when loaded across layers. This is indicative of good printing technique with no presence of cold joints.

In order to avoid the normalisation of dimensions, the same sets of specimens were analysed using the calculation of work of fracture. Work of Fracture is an indicator of the crack resistance of the specimens upon loading. This is calculated using the least R-squared method from the area of the curves under the load vs crack-opening displacement graph. Considering that a displacement control method of loading has been employed, the failure of the specimens is very gradual. The work of fracture is normalised by the ligament area (product of width and effective depth of each specimen) to obtain the fracture energy which is a material parameter represented in N/m as studied and developed by Bažant et al (1984) [11, 12]. These fracture energy values are plotted in Fig 4.

The micro-pores in the top layers of the printed elements remain and solidify during the printing process whereas those in the bottom layers are consolidated and lost after the subsequent layers are added on top. These micro-pores act as barriers for crack propagation allowing for a higher energy release during the fracture. This phenomenon precipitates in the slightly higher fracture energy and flexural capacity of the specimens taken from the top compared to those taken from the bottom of a printed element. The printed specimens loaded vertically fail with the crack propagating along the printing path resulting in a much more brittle failure and results in poor flexural capacity due to a poor crack resistance. The cast elements also have a higher proportion of voids compared to the printed elements due to the additional compaction of the printed elements in the extrusion process. This allows for an even higher crack path resistance compared to that of the printed elements and therefore a higher fracture energy compared to that of the printed elements. It is therefore seen that while the same mix design of the cementitious mortar is employed in the printing process and the casting process, the printing process itself and the orientation of the specimens can have a significant influence on the material parameters such as the flexural capacity and fracture energy. This also implies that despite the presence of weaker interfaces between layers, the printed specimens on average offered a similar resistance to load as the monolithically cast counterparts. Therefore understanding the influence of interfaces becomes even more paramount to an effective design process.

3 NUMERICAL MODELLING USING ABAQUS AND VALIADTION OF RESULTS

Concrete Damage Plasticity (CDP) model has been developed using ABAQUS software to understand the influence of interfaces on the load capacity in 3-point bending tests. The parameters such as the dilation angle, eccentricity and poisson's ratio are taken from a collection of similar studies involving fracture in 3D printed materials [13, 14]. For the purpose of this study the viscosity parameter has been chosen as 5×10^{-7} after an iterative procedure to identify the appropriate residual capacity of specimens. The complete set of parameters used as input for the CDP model are shown below in Table 1.

To understand the influence of the interfaces, separate interface elements with 1mm thickness are modelled in between the layers of 9 mm which contain the bulk materials. All the elements are bonded to each other with a tie constraint always maintaining the relative strain between the layers equal to 0. The load conditions used in the model can be seen below in Fig 5.

A linear geometric triangular mesh consisting of (CPE3) 3-node linear plane strain triangle elements as shown below in Fig 6 has been employed to discretize the specimen geometry. The mesh is structured with an element size of 0.5 mm at the interface. A higher density of the mesh is employed close to the perceived crack with an element size of 0.5 mm. Both the layers and the interface parts are given the same geometrical effective length of 160 mm same as the size of the specimens tested in 3-point bending.

In the case of the monolithically cast specimens to avoid the presence of interfaces, both the interface elements and the layer elements were assigned the same constitutive properties. The compressive constitutive behaviour is approximated based on estimates from the fib Model Code (2010) for a compressive strength of 70 MPa. The tensile constitutive behaviour of concrete used in the case of monolithically cast elements is depicted in Fig 7 with an equivalent tensile stress (σ_{ct}) vs crack opening (w) curve. The area under the bilinear curve is calibrated to the fracture energy (G_F). It can be noted that for the case of monolithically cast elements, the equivalent tensile strength of 5.54 MPa and an equivalent G_F of 144 N/m has been employed. The G_F value has been taken from the average fracture energy in the case of printed elements taken from the top with a layer orientation perpendicular to the direction of loading. The equivalent tensile stress has been computed based on the Flexural tensile strength suggestion of the fib Model Code (2010) from a flexural capacity of 8.4 MPa in 3-point bending as written below.

$$\sigma_t = \frac{0.06h^{0.7}}{1+0.06h^{0.7}}\,\sigma_f \qquad (2)$$

To avoid the mesh dependence of the model, the CMOD in the constitutive model is divided by a characteristic length (equivalent to the mesh size) to obtain an equivalent strain.

As can be seen from the localisation of plastic strain shown in Fig 8, the crack is localised at the notch at the centre of the specimens. Upon computing the Load vs CMOD response from the resulting ABAQUS model, it can be seen in the Fig 9 that there is a good agreement between the experimental results and the ABAQUS model in the case of cast elements.

To simulate the presence of interface elements in the printed specimens, the interface elements have been chosen to have a poorer tensile constitutive property. Specifically, the tensile constitutive property equivalent of the flexural tensile strength of vertical specimens has been utilised. The equivalent tensile strength of 1.54 MPa based on the fib model code (2010) for a flexural tensile strength of 3.5 MPa and an equivalent G_F of 40 N/m computed from the vertical specimens is employed. The tensile constitutive properties of the interface elements and the layer elements are depicted in the Fig 10.

It can be seen from Fig 11 that upon reducing the tensile constitutive properties of

the interface elements, a good agreement can be achieved in the Load vs CMOD results of the experimental and ABAQUS models.

4 CONCLUSIONS

It can be established from Figs 2, 3 & 4 that there is clear orthotropy in the properties of printed elements. The printed elements tested with layer orientations parallel to the direction of loading have a much weaker mechanical performance compared to the elements tested with layer orientation perpendicular to the direction of loading. This indicates a presence of weak interfaces between the layers. While there are no direct methods to establish the mechanical properties of these interfaces such as the tensile strength and the fracture energy, the ABAQUS model can estimate the properties using a comparison between the properties of the printed elements and the monolithically cast elements. The vertical elements are characterised by the weak interfaces and therefore it can be said that the limiting constitutive properties such as the tensile strength and the fracture energy of the interface are that of the printed elements tested with direction of loading parallel to the layer orientation. In this case the tensile strength of the interface is 1.54 MPa and the fracture energy of the interface is 40 N/m, whereas the tensile strength of the monolithically cast specimens and the printed elements, characterised by the layer elements (bulk material) is 5.54 MPa and the fracture energy of the layer elements is 144 N/m.

The following correlation can therefore be established:

$$\frac{\sigma_{interface}}{\sigma_{layer}} = \frac{G_{f,interface}}{G_{f,\ layer}} = 0.277$$

It can also be noted that the printed elements tested with layer orientations perpendicular to the direction of testing have the same mechanical properties as that of the monolithically cast elements of similar dimensions. This establishes that the printing quality is maintained despite the presence of weak interfaces which are unavoidable when the elements are loaded across the interfaces. The presence of interfaces acts as barriers to crack propagation offering a higher resistance to fracture and thus can be utilised to augment the performance of printed elements.

REFERENCES

[1] Wangler, T., Lloret, E., Reiter, L., Hack, N., Gramazio, F., Kohler, M., Bernhard, M., Dillenburger, B., Buchli, J., Roussel, N. and Flatt, R.J., 2017. Digital concrete: opportunities and challenges. *Rilem Technical Letters*, 1(1), pp.67-75.

[2] Mohan, M.K., Rahul, A.V., De Schutter, G. and Van Tittelboom, K., 2021. Extrusion-based concrete 3D printing from a material perspective: A state-of-the-art review. *Cement and Concrete Composites*, 115, p.103855.

[3] Liu, C., Yue, S., Zhou, C., Sun, H., Deng, S., Gao, F. and Tan, Y., 2021. Anisotropic mechanical properties of extrusion-based 3D printed layered concrete. *Journal of Materials Science*, 56(30), pp.16851-16864.

[4] De Schutter, G., Lesage, K., Mechtcherine, V., Nerella, V.N., Habert, G. and Agusti-Juan, I., 2018. Vision of 3D printing with concrete—Technical, economic and environmental potentials. *Cement and Concrete Research*, 112, pp.25-36.

[5] Sanjayan, J.G., Nematollahi, B., Xia, M. and Marchment, T., 2018. Effect of surface moisture on inter-layer strength of 3D printed concrete. *Construction and Building Materials*, 172, pp.468-475.

[6] Nerella, V.N., Hempel, S. and Mechtcherine, V., 2019. Effects of layer-interface properties on mechanical performance of concrete elements produced by extrusion-based 3D-printing. *Construction and Building Materials*, 205, pp.586-601.

[7] Emmons, P.H., 1992. *Concrete repair and maintenance illustrated: problem analysis; Repair Strategy; Techniques (Vol. 28).* John Wiley & Sons.

[8] Le, T.T., Austin, S.A., Lim, S., Buswell, R.A., Law, R., Gibb, A.G. and Thorpe, T., 2012. Hardened properties of high-performance printing concrete. *Cement and Concrete Research*, 42(3), pp.558-566.

[9] Marchment, T. and Sanjayan, J., 2019. Method of enhancing interlayer bond strength in 3D concrete printing. In *First RILEM International Conference on Concrete and Digital Fabrication–Digital Concrete 2018 (pp. 148-156).* Springer International Publishing.

[10] Julio, E.N., Branco, F.A. and Silva, V.D., 2004. Concrete-to-concrete bond strength. Influence of the roughness of the substrate surface. *Construction and Building Materials*, 18(9), pp.675-681.

[11] Bažant, Z.P., 1984. Size effect in blunt fracture: concrete, rock, metal. *Journal of Engineering Mechanics*, 110(4), pp.518-535.

[12] Bažant, Z.P. and Li, Z., 1996. Zero-brittleness size-effect method for one-size fracture test of concrete. *Journal of Engineering Mechanics*, 122(5), pp.458-468.

[13] Dias-da-Costa, D., Alfaiate, J. and Júlio, E.N.B.S., 2012. FE modeling of the interfacial behaviour of composite concrete members. *Construction and Building Materials*, 26(1), pp.233-243.

[14] Tang, T., Yang, S. and Zollinger, D.G., 1999. Determination of Fracture Energy and Process Zone Length by Using Variable-Notch One-Size Specimens. *Materials Journal*, 96(1), pp.3-10

Dilation angle	Eccentricity	σb0/σc0	Kc	Viscosity parameter	Poisson's ratio
30	0.1	1.16	0.667	5E-07	0.2

Table 1: Parameters used in the CDP model in ABAQUS

Figure 1: 3-point bending test setup with a clip-guage at the notch-tip to control CMOD.

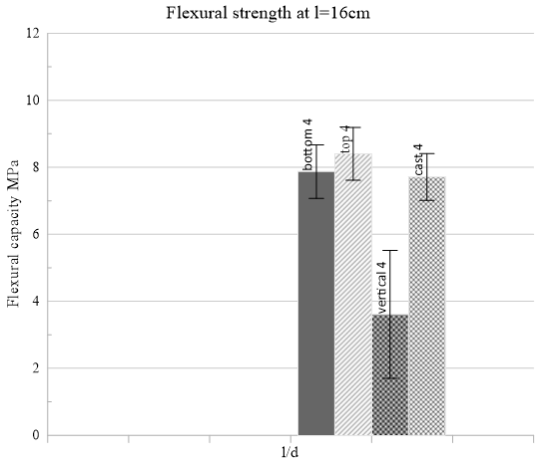

Figure 2: Nominal flexural strength for cast and printed specimens

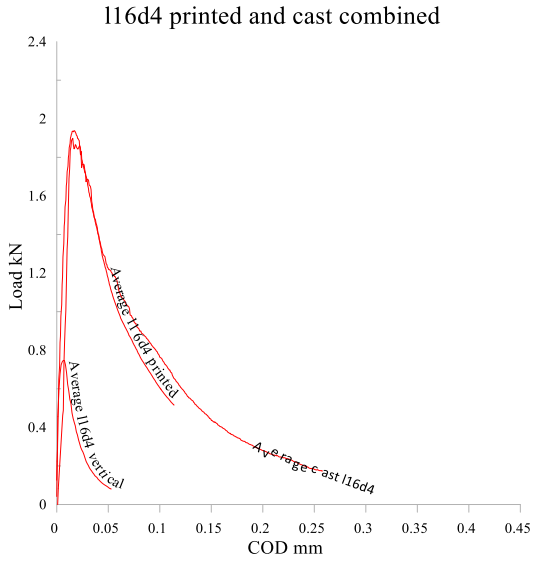

Figure 3: Average of Load vs COD curves of printed and cast specimens

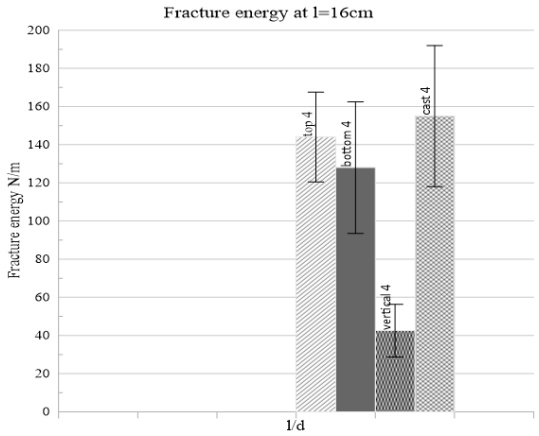

Figure 4: Average Fracture energy of printed and cast specimens

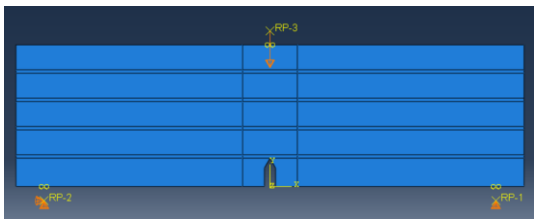

Figure 5: 3-point bending model with interfaces elements represented along with the loads

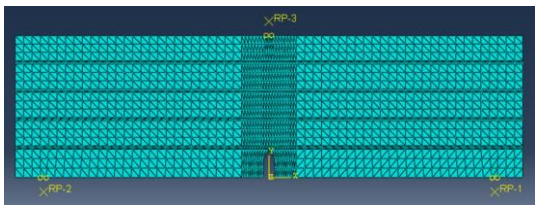

Figure 6: CPE3 plane strain mesh with denser mesh close to the notch and interface elements

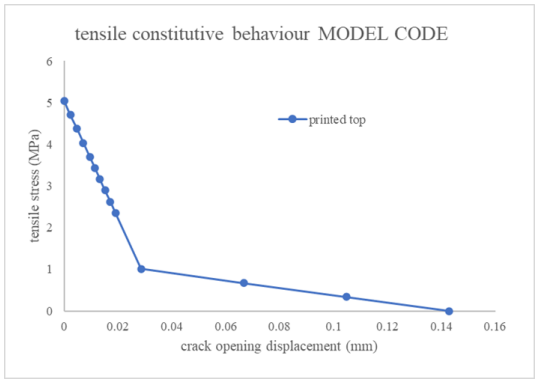

Figure 7: Tensile constitutive property

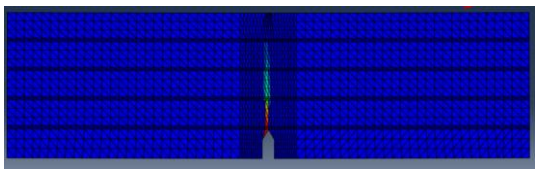

Figure 8: Crack in 3-point bending characterised by plastic strain in X-direction

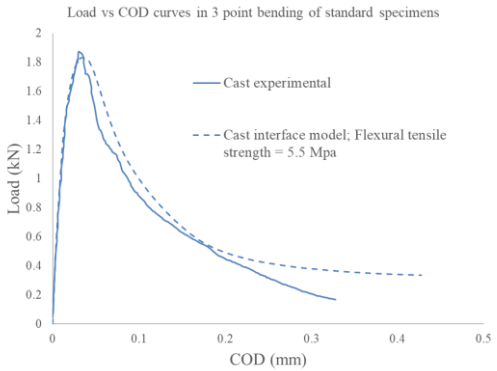

Figure 9: Agreement between the experimental results and ABAQUS model in case of monolithically cast specimens

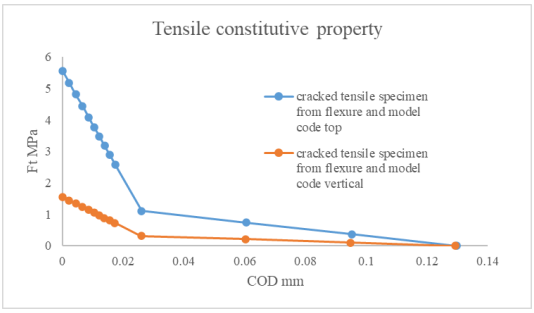

Figure 10: Tensile constitutive property of layer and interface elements

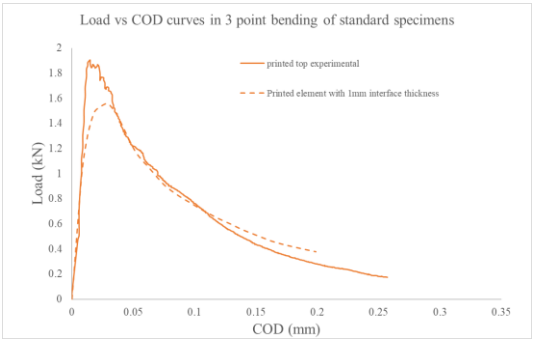

Figure 11: Agreement between the experimental results and ABAQUS model in case of printed element